RSC Advances

PAPER

View Article Online
View Journal | View Issue

Cite this: *RSC Adv.*, 2017, **7**, 9115

Evaluation of a chloroaluminium phthalocyanine-loaded magnetic nanoemulsion as a drug delivery device to treat glioblastoma using hyperthermia and photodynamic therapy†

L. B. de Paula,[a] F. L. Primo,[b] M. R. Pinto,[c] P. C. Morais[de] and A. C. Tedesco*[a]

Received 31st October 2016
Accepted 21st January 2017

DOI: 10.1039/c6ra26105a

rsc.li/rsc-advances

This study reports the production of magnetic nanoemulsions (MNEs) loaded with citrate-coated maghemite nanoparticles (0.15×10^{16} or 1.50×10^{16} particle per mL) and chloroaluminum-phthalocyanine (0.05 mg mL^{-1}). Using different cell line models (BM-MSC, U87MG, and T98G) an *in vitro* test was performed to assess the cell viability while incubating the cells with the two prepared formulations, before and after performing hyperthermia (HPT: 1 MHz frequency, 40 Oe magnetic field amplitude) and photodynamic therapy (PDT at 670 nm wavelength, 700 mJ cm^{-2} energy density). We found from all cell lines that under the HPT treatment the cell viability reduction has averaged 15%, regardless the magnetic nanoparticle content within the MNE. Using both MNE formulation (0.15×10^{16} or 1.54×10^{16} magnetic particle per mL) and applying only PDT light treatment we reach an average decrease of 52%. However, a total reduction of about 70% was found while combining the HPT and PDT treatments. Confocal studies clearly indicated the cytoplasm localization and active site of the drug delivery device. Therefore, the combined treatment of HPT and PDT represents a promising paradigm for brain cancer intervention, such as glioblastoma.

Introduction

Brain tumors known as glioma are the most common neoplasms found in the central nervous system (CNS) of adults. According to the World Health Organization, the tumor classified as glioblastoma multiforme (GBM) is the most aggressive and common type of glioma.[1] Some distinct features of GBM are the atypical nucleus, rapid growth, microvascular proliferation, necrosis, genetic instability and resistance to chemotherapeutic agents,[2] all of which may lead to unfavorable prognosis and an average survival of approximately one year for all affected patients.[1,2] GBM is associated with uncontrolled cell proliferation, remarkable invasiveness and multiple genetic alterations, so any alternative treatment is leading to eradicate GMB is desirable.[3] However, as the poor survival rate indicates, radiotherapy and chemotherapy (temozolomide – TMZ) treatments have not been effective in preventing disease progression. Standard care treatment of tumors such as glioblastoma includes maximal surgical resection of the tumor followed by radiotherapy and chemotherapy (TMZ). At the same time, neoplasms with abnormal cells not infiltrating the adjacent CNS tissue can represent a risk to patients, as they are difficult to treat and also proliferate very quickly.[1] The therapeutic approach adopted to treat newly diagnosed malignant gliomas has mostly remained unchanged for decades, consisting of surgical removal of the tumor mass (as much as possible) followed by concomitant radiotherapy and chemotherapy.[1] However, glioma cells have exhibited resistance to radiation and chemotherapy,[4] not to mention that low tumor tissue selectivity and blood-brain barrier (BBB) perfusion have limited glioblastoma chemotherapy.[5] We demonstrated the application of our nanocarriers would then surgical resection followed by the combination of hyperthermia and photodynamic therapy. Thus, ensure minimal loss of healthy tissue and preserve the patient's life.

In a brain cancer tumor, cancer stem cells (CSCs) represent a small fraction of the total cancer cell population.[6] The CSCs represent a unique subset of tumor cells thought to play a critical role in the initiation and progression of carcinogenesis.[7]

[a]*Department of Chemistry, Center of Nanotechnology and Tissue Engineering – Photobiology and Photomedicine Research Group, Faculty of Philosophy, Science and Letters of Ribeirão Preto, University of São Paulo, 14040-901 Ribeirão Preto, SP, Brazil. E-mail: atedesco@usp.br*

[b]*São Paulo State University (UNESP), School of Pharmaceutical Sciences, 14801-903, Araraquara-SP, Brazil. E-mail: flprimo@fcfar.unesp.br*

[c]*Department of Chemistry, Laboratory of Enzymology, Faculty of Philosophy, Science and Letters of Ribeirão Preto, University of São Paulo, 14040-901 Ribeirão Preto, SP, Brazil*

[d]*Institute of Physics, University of Brasilia, 70910-900 Brasília, DF, Brazil*

[e]*College of Chemistry and Chemical Engineering, Anhui University, 230601 Hefei, China*

† Electronic supplementary information (ESI) available. See DOI: 10.1039/c6ra26105a

This subset of CSCs has subsequently been shown to express consistent proliferation, self-renewal, and differentiation characteristics.[8] Due to their unique replicative characteristics, the CSCs are broadly hypothesized to initiate and drive tumor growth and recurrence, while other non-CSC bulk tumor cells are largely incapable of such extended expansion.[7–9] Since the initial studies proposing the presence of this unique subpopulation some reports have subsequently demonstrated the presence of CSCs responsible for tumorigenesis in various malignancies such as breast, colon, ovarian, pancreatic, melanoma, multiple myeloma and brain cancers.[8] Studies have suggested similarities of CD133+ CSC with the proneural subtype and of CD133 CSC with the mesenchymal subtype.[10] Additionally, studies have shown that a small population of CSCs accounts for tumor/glioma growth, resistance, and recurrence.[3,6,9] Development of specific therapies addressed to target the CSCs creates the possibility of improving cancer patient's survival and quality of life.[6,9] Many strategies have been developed to overcome the therapeutics difficulties, among them drug delivery nanosystems have been produced to target therapeutic agents and improve their biodistribution and therapeutic index in the tumor. These new material systems include a polymer or lipid-based carriers such as liposomes, polymeric nanospheres and nanocapsules, micelles and dendrimers, and inorganic nanomaterials.[11]

Cancer treatment and diagnosis based on nanotechnology approaches have revolutionized conventional medicine in the past few years.[12,13] Theranostic drugs have gained prominence in many procedures, allowing for both diagnosis and treatment of neoplastic diseases.[14] In this scenario, nanoparticles (NPs) and in particular nanoemulsions (NEs), have the potential to improve the therapeutic concentration of drugs in the target tissue, thus increasing drug efficacy while reducing drug toxicity and side effects and achieving steady-state drug therapeutic levels over prolonged periods.[15]

NEs have unique properties such as small droplet size, exceptional stability, transparent appearance and rheology.[16] NEs have been used in most forms of drug delivery for topical, ocular, intravenous, internasal and oral delivery. Such applications assist in solvation process of water-insoluble drugs given which NEs have a lipophilic nature. The new rheology properties of the NEs formulations help to formulate solutions aqueous of different actives that can be easily delivered to patient.[16] NEs can be used as building blocks for the preparation of more complex materials due to their small size, high stability and high surface area that allow the easy association of a liquid–liquid surface with functional parts such as designer macromolecules.[16] The method of preparation of nanoemulsions with reproducible properties and small droplet sizes seen being used as a low-energy process. The use of this process has been a field of growing interest.[17–19]

Low-energy methods make use of accessible phase transitions occurring during the emulsification process as a result of changes in surfactant film spontaneous curvature.[17,18] This curvature transition has been achieved through different routes described by four basic process: (a) partitioning of alcohol from the oil to the aqueous phase or diffusion of water into the initial droplet, both producing a shift from lipophilic to hydrophilic conditions; (b) chemical reactions which convert lipophilic surfactants to hydrophilic surfactants;[17,20,21] (c) a sudden decrease of ionic strength with ionic surfactant systems[17,22,23] and (d) an increased hydration of poly(oxyethylene) chains of PEOtype nonionic surfactants.[17] These processes of reversing the spontaneous curvature water-in-oil to an oil-in-water configuration reduce the solubility capacity of oil to such an extent that supersaturation may occur, leading to oil droplets nucleation.[17]

Emulsion polymerization is perhaps the best-known example in polymer synthesis where hydrophobic monomers contained in droplets are polymerized to create polymeric particles. NEs have been utilized extensively in polymer synthesis.[16]

Multifunctional NPs[24,25] aimed at tissue microenvironments open new possibilities for basic research while help to understand complex issues associated with tumor progression, angiogenesis, and metastasis.[12] However, the design principles underlying nanotherapeutics and theranostic protocols remain a challenge.[14] Additionally, different mechanisms can fade out or eliminate NPs, preventing them from reaching the target site in the body. Moreover, these nanomaterials need to reach tumors or cancer cells in circulation to perform their therapeutic function as an advanced drug delivery system, gene therapy, or combined therapy system.[12] Combination therapy which uses two or more kinds of drugs with different mechanism of action has recently gained much attention as a new trend in the field of nanomedicines.[26]

A promising strategy points to the use of surgical hyperthermia (HPT) protocols, being HPT a therapeutic procedure that firstly exposes tumor sites to magnetic nanoparticles (MNPs) for subsequent application of an external AC magnetic field, the latter causing a small rise in the tumor temperature (say 2 to 4 °C) triggering the cancer cell death by activating the apoptotic pathway.[27] The principle relies on the fact that small changes in the cell tumor temperature can halt tumor progression and destroy the tumor cells.[28] At the cell membrane level, HPT promotes changes that reduce transmembrane transport and destabilize the membrane potential.[24,29,30]

Zaki *et al.* examined mechanisms of action of anticancer silver and gold complexes were not DNA they act mainly by targeting mitochondrial membrane of a cancer cell or by inhibiting through thiol-containing proteins/enzymes, such as thioredoxin reductase.[31]

The combination of HPT with radiation and anticancer agents has been used clinically and has shown positive results to a certain extent.[32] To Ahmed *et al.* the clinical results of HPT treatment alone have been only partially satisfactory. Cell death following HPT treatment is a function of both temperature and treatment duration.[32]

HPT is known to induce apoptosis in cancer cells.[32] Blocking of this defense mechanism promotes aberrant cell proliferation and accumulation of genetic defects, which eventually result in tumorigenesis.[32] In the apoptotic mechanism, the caspases have central and essential functions. There are three pathways for the activation of caspases: the intrinsic or mitochondrial pathway, the extrinsic pathway or the death receptor, and the

newly described but less understood endoplasmic reticulum pathway.[32]

Although heat shock has been studied for decades, the precise mechanism of HPT-induced apoptosis has not yet been fully elucidated.[32]

Studies in a rat glioma model have successfully established that HPT is safe and efficient.[30] Indeed, the use of the HPT to treat tumors like GBM may reduce tumor size and stop the progression of the GBM levels III and IV. This approach could improve the way for safer surgical procedures to extract the tumor mass within a more restricted area, thereby damaging the surrounding healthy tissue minimally. Furthermore, with the surgical field open (during surgery) the surrounding healthy tissue, impregnated with photosensitizing (PS) molecules, could be efficiently treated using photodynamic therapy (PDT). This therapeutic approach involves three essential components, namely a PS-drug (already impregnated into the tissue), exposure the area to specific visible light, and oxygenation (usually O_2 dissolved in the tissue) to activate the drug.[33] The PDT pathways would generate a cascade of events including apoptotic and necrotic cell death in both the tumor and the neovasculature, leading to a permanent lesion and destruction of the GBM cells that remained in the healthy tissue.[29] Dereski *et al.* found that the effects were greater than additive when HPT was given post-PDT.[34] Hyperthermic temperatures were found to inhibit repair of sub-lethal damage thereby making hypoxic cells more sensitive to PDT. Using a murine mammary adenocarcinoma model Chen *et al.* showed that the combination of PDT and HPT produced a synergetic tumor response.[24] Hirschberg *et al.* examined synergistic effects of 5-aminolevulinic acid-mediated PDT and HPT concurrently on human and rat glioma spheroids.[35] The results showed that when administered separately PDT and HPT were not very effective. However, concurrent administration of the two treatment modalities (HPT and PDT) resulted in significant toxicity enhancement. Therefore, we envisage that the combination of these two approaches could become a valuable tool to work synergistically to treat GBM with minimal side effects. It could promote significant tumor regression while extending the lifetime of patients with a high level of glioma progression. In this context, the present study describes the development of an innovative magnetic nanoemulsion loaded with citrate-coated maghemite nanoparticles and chloroaluminum-phthalocyanine (Fig. 1) and the *in vitro* studies using glioblastoma, bone marrow mesenchymal stem cells and fibroblast murine cell lines while combining the use of HPT and PDT therapies. Worth mentioning that citrate-coated maghemite nanoparticles have been reported as biocompatible.[36]

Furthermore, a preliminary *in vitro* test of magnetic nanoemulsions loaded with citrate-coated iron oxide nanoparticles and chloroaluminum-phthalocyanine using one cell line model (human bone marrow stromal).[37] However, in this preliminary study the magnetic nanoemulsion was loaded with a very low concentration of MNPs (0.15 to 1.50 $\times$ 10^{13} particle per mL), which is three orders of magnitude lower than the present report (0.15 to 1.50 $\times$ 10^{16} particle per mL). Finally, as described in the next section, three different cell lines (BM-MSC, U87MG, and T98G) were included the present study, including the tumorigenic U87MG, thus allowing a comprehensive evaluation of the HPT and PDT therapies' efficacy and their synergism.

Results and discussion

Nanoemulsification (o/w type) provides MNEs with superior thermodynamic stability as pointed out by Primo *et al.* while describing their physicochemical properties.[27] The oil phase in the NE's core offers an optimal chemical environment to host phthalocyanine compounds with lipophilicity properties. The NEs can also incorporate magnetic material at the desired final concentration to produce MNEs precisely designed to perform biological functions. Spectroscopy studies carried out under steady-state condition showed ClAlPc absorption spectral profiles almost unchanged after incorporation within the MNE/ClAlPc samples (Fig. 2), in agreement with the picture of the intramolecular interaction between the drug and the polymer micro-heterogeneous environment of the formulation.[27] The electrostatic repulsion between oil droplets explains the enhanced colloidal stability of the as-produced samples while preventing particle flocculation and coalescence.

Particle size analysis showed that all colloidal formulations produced in the present study and containing NE/ClAlPc were in the nanoscale size, with typical mean diameter around 220 $\pm$ 20 nm and size distribution value (PdI) of 0.25. TEM micrographs of the NE/ClAlPc (0.025 mg mL^{-1}) sample

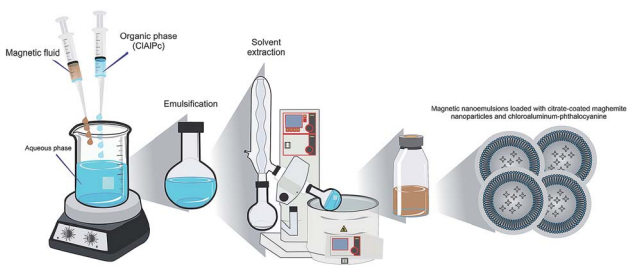

Fig. 1 Schematic representation of MNE/ClAlPc preparation.

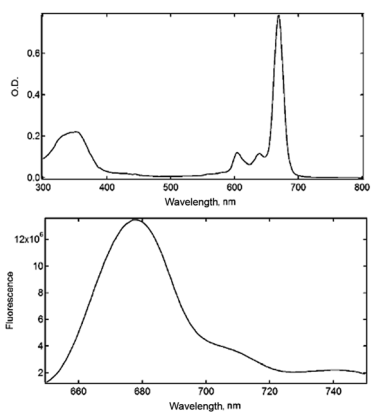

Fig. 2 MNE/ClAlPc absorption spectrum in the UV-visible to 300–800 nm range (A); and (B) MNE/ClAlPc fluorescence emission spectrum under excitation at 610 nm and emission at 675 nm (slits = 10 nm/ex, 10 nm/em; integral time = 0.1, 450 W).

revealed approximate spherical shape with 250 nm mean diameter (Fig. 3). Electrophoresis mobility measurements allowed determination of the zeta potential with a mean value of −56 mV. Formulations containing highly charged particles, with positive or negative potential values (greater than +30 mV or lower than −30 mV), are frequently acknowledged as stable. The formulations were stored at 4 °C for 90 days. Our findings demonstrate excellent physical and chemical stability of MNE with a size less than 200 nm, exhibiting a narrow size distribution (PI index less than 0.2) and the zeta potential higher around |40| mV.

The LumiSizer® is a device that analyses these dispersions and enables prediction of the stability (shelf life) of several pharmaceutical formulations, such as suspensions and emulsions.[38] Other researchers assessed a quite new method to evaluate the colloidal dispersion of suspensions is through the application of a centrifugal field. The analytical centrifuge is an effortless and undemanding method that allows for estimating the shelf life of suspensions A centrifuge field allows the acceleration of the demixing phenomenon, evaluating the change in concentration by detecting the transmission profiles along the entire height of the sample.[39] This technique can measure the stability of formulations up to 2.300 times faster than conventional tests.[38]

ClAlPc nanocapsules formulations obtained from the factorial design were submitted to storage stability test at 4 °C for 12 months. Both particle size and zeta potential as a function of time were used as stability indices of colloidal systems during this evaluation. These structural parameters of the particles are closely associated with the onset of stability loss in dispersed systems which may result in the following instability processes: flocculation, creaming, molecular diffusive transfer (Ostwald ripening), or coalescence.[28]

The separation process of the nanoparticle systems was previously evaluated by monitoring the changes in the profiles caused by cremosity, sedimentation or flocculation. The transmission profiles of empty formulations of NE/ClAlPc, not associated and related to additives showed no substantial changes in the transmission profiles as expected.[38]

These results were indicating that the particles demonstrated to be homogeneous over the entire experiment, and no destabilization processes were observed. These results show the formulations stability for a time period up to 6 months at 25 °C.

The *in vitro* studies herein described using the MNE/ClAlPc samples rely on the BM-MSC, U87MG and T98G biological models. Fig. 4 illustrates the BM-MSC, U87MG and T98G cells in the typical confluent stage (three days culture). Cells display plastic adherent properties under normal culture conditions and show fibroblast-like morphology (Fig. 4A and B). Glioblastoma (U87MG and T98G) shows epithelial morphology (Fig. 4C–F), which underlines its high level of aggressiveness a highly malignant lesion with poor prognosis. GBMs are characterized by rapid cell proliferation and aggressive invasion and destroy of the surrounding healthy brain tissue.[40] In our tests, we found that the cells internalized the MNE/ClAlPc samples after 3 h incubation at 37 °C.[37]

The results in Fig. 5 indicated that the cell uptake was kept at the cytoplasmic level only because of the MNE/ClAlPc homogeneous distribution after the incubation. PS localizing in cytoplasmic or mitochondria generally leads to the loss of membrane permeability and release of pro-apoptotic mediators.[41] Cytotoxicity assay (MTT test)[42] was conducted with the MNE/ClAlPc samples at the two distinct MNP concentrations (0.15 and 1.50 × 10^{16} particle per mL) while keeping fixed the ClAlPc concentration (0.5 μmol L^{-1}). The results showed in Fig. 6 reveal the biocompatibility of the nanomaterial and the absence of cell death. *In vitro* studies based on magnetic targeting have been widely applied in biological investigations including cell separation and enrichment, gene transfection and cell population detection assays.[43]

Muehlmann *et al.* also showed that ClAlPc internalization into cancerous and non-cancerous cells occurred in the cytosol

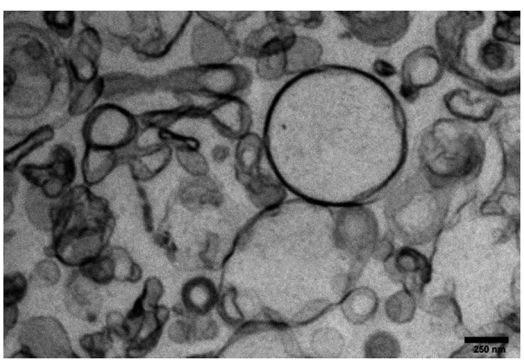

Fig. 3 Morphological analysis by TEM of NE/ClAlPc loaded at 0.025 mg mL^{-1}. High-resolution at 70 kV and an increase of 44 000×.

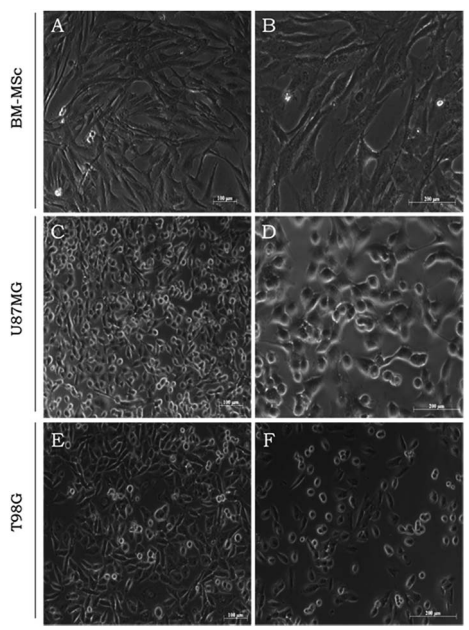

Fig. 4 Morphology of the cell lines obtained by phase contrast microscopy under a Carl Zeiss microscope. BM-MSc, U87MG and T98G cell controls in α-MEM and DMEM/FBS 10% at 72 h stage (A, C and E) 10× and (B, D and F) 20×.

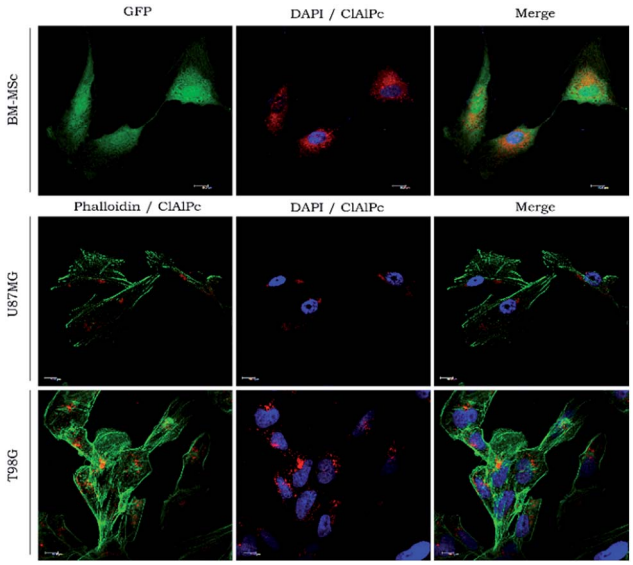

Fig. 5 Confocal laser scanning microscopy regarding the *in vitro* uptake of the photosensitive drug in the nanocarrier (MNE/ClAlPc). BM-MSC cells: GFP (green fluorescent protein) – expressed constitutively, U87MG and T98G cells: Alexa Fluor 488 phalloidin labeling of actin filaments; DAPI (blue) – tagging nuclear; ClAlPc (red) – tagging the NE/ClAlPc. Scale bar 10 μm.

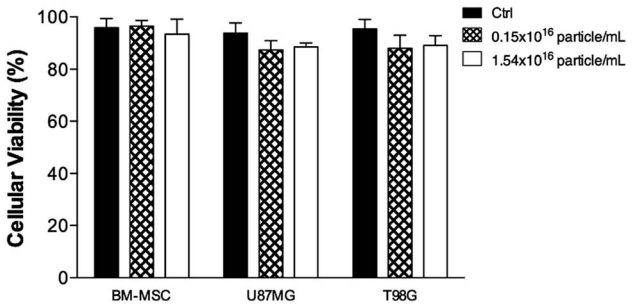

Fig. 6 Viability of the cells lines incubated with the as-produced MNE/ClAlPc in the absence of HPT and PDT. Ctrl – control (cells in medium at 3% serum). There was no statistical difference in the experiment. All data were expressed as the mean ± SEM of three independent experiments.

of the cells.[44] This finding may represent an advantage as it could trigger the HPT or PDT process in organelles like lysosomes or mitochondria while protecting the nucleus or mutagenic side effects in healthy cells. It would also generate a particular mechanism of cell death[44] for the remaining cancer cells thereby protecting healthy tissue after tumor removal. Worth mentioning that in our protocol, we used HPT at the same time we employed the nanocarrier containing the PS for photoactivation, allowing to activate the PS-drug in step following HPT optically. The magnetic mobility and heating capability of magnetic nanoparticles can also help to trigger cellular events *in vivo*,[45] thus inducing an active immunological response that may enhance the outcome of the whole process. The fact that HPT combined with PDT-induced MSC cell death (CSCs cell type) reinforced the idea the MNE/ClAlPc formulation is potentially applicable to treat glioblastoma while avoiding negative results of CSC.[6] It is well established that MNPs induce cancer cell death and destroy the tumor tissue, but studies on the use of HPT therapy in brain gliomas are scarce.[30] Recent studies have shown that MNEs can also be utilized for the controlled delivery of therapeutic agents.[27]

Fig. 7 indicates the effect of HPT only and the combined result of HPT and PDT therapies on the biological response of

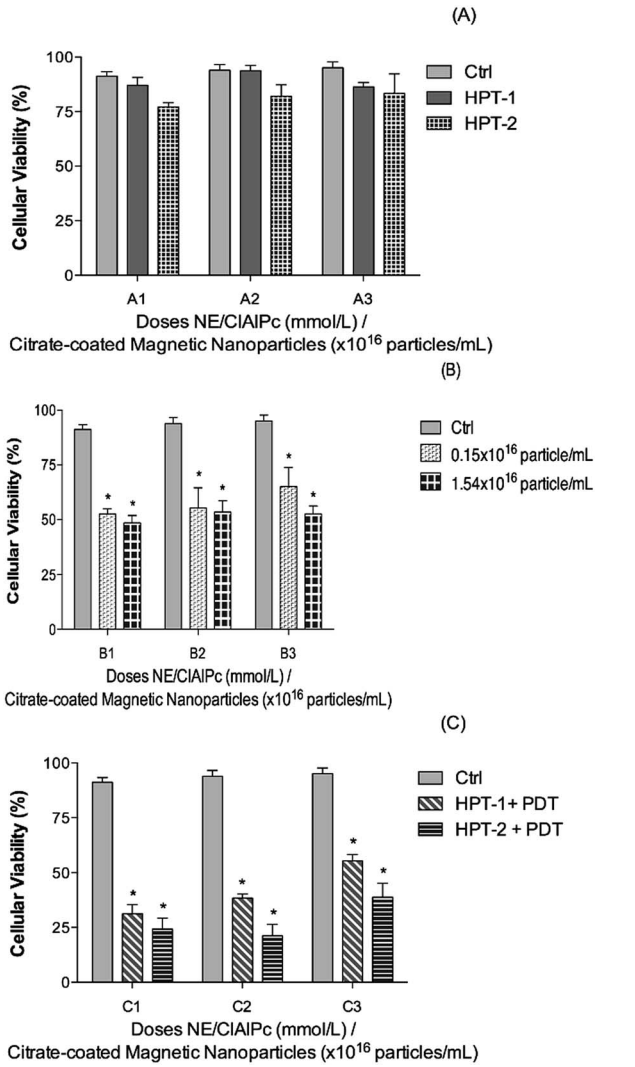

Fig. 7 Viability of cell lines incubated at 3 hours with different MNE containing equal contents of encapsulated ClAlPc (0.5 mg mL^{-1}). Ctrl: control (cells in 3% serum medium); (A) – A1: BM-MSc; A2: U87MG and A3: T98G; HPT: hyperthermia treatment; HPT-1: 1 MHz/40 Oe + sample containing 0.15×10^{16} magnetic nanoparticle per mL; HPT-2: 1 MHz/40 Oe + sample containing 1.54×10^{16} magnetic nanoparticle per mL. (B) – B1: BM-MSc; B2: U87MG and B3: T98G; only evaluation of photodynamic therapy (700 mJ cm^{-2}). (C) – C1: BM-MSc; C2: U87MG and C3: T98G; PDT: photodynamic therapy (700 mJ cm^{-2}); HPT-1 + PDT: sample containing 0.15×10^{16} magnetic nanoparticle per mL + 700 mJ cm^{-2}; HPT-2 + PDT: sample containing 1.54×10^{16} magnetic nanoparticle per mL + 700 mJ cm^{-2}. Statistical analysis was performed by one-way analysis of variance (ANOVA) and Tukey test. All data were expressed as the mean ± SEM of three independent experiments. Statistical significance for this study was considered at $*p < 0.05$.

different cells. We found that while applying the HPT treatment using the MNE/ClAlPc formulation the cell viability is slightly reduced in all the biological models employed regardless the MNP concentration, as shown in Fig. 7A (columns A1/HPT-1 and A1/HPT-2; A2/HPT-1 and A2/HPT-2; A3/HPT-1 and A3/HPT-2). Differently, while using the MNE/ClAlPc formulation (containing 0.15×10^{16} and 1.50×10^{16} magnetic particle per mL) in the PDT treatment (see Fig. 7B) we found (compared to the control group) an average 52% of cell death. There was no significant difference compared between the two concentrations of the formulation. Finally, compared with the data shown in Fig. 7A and B the data illustrated in Fig. 7C clearly evidenced the synergism of the combined HPT and PDT treatments, revealing an increase of up to 70% in cell death. The results have not been shown. However, the light only does not cause in cell death. Silva *et al.* using the glioblastoma grade IV (U87MG) cell line demonstrated that the laser irradiation did not result in cell death.[38] Despite the excellent synergism achieved while combining HPT and PDT treatments we found that in the range of our experiment, the therapeutic outcome did not depend strongly upon the MNP content within the MNE/ClAlPc samples (see Fig. 7C). Nevertheless, the cell death increased on the basal level of the control (BM-MSCs, U87MG, and T98G) while increasing the MNP content within the MNE/ClAlPc samples from 0.15×10^{16} to 1.50×10^{16} particle per mL. Compared with the control (see Ctrl column in Fig. 7) and considering the combined HPT and PDT treatments we found that the mitochondrial activity is strongly correlated with the activation of cell death mechanisms. Moreover, the treatment of the assayed cells with the MNE/ClAlPc samples enabled *in vitro* cell imaging and monitoring of the MNE/ClAlPc uptake by the cell lines with confocal microscopy while allowing simultaneous monitoring of the magnetic material. The precise localization of the tumor using the fluorescent properties of ClAlPc would guide not only the surgical procedures but also allows the use of the PDT by visible light activation to induce apoptotic and/or necrotic action on the remaining glioma cells. Furthermore, in clinical applications it also offers an extra safety margin after the surgery, thus providing for instance a more comprehensive brain cancer treatment. The approach regarding the combination of HPT and PDT, with its synergistic outcome, could be more efficient in a successful treatment of glioblastoma.

Experimental

Magnetic nanoemulsions

Magnetic nanoemulsions (MNEs) loaded with magnetic nanoparticles (MNPs) plus photoactivated drugs, such as chloroaluminum phthalocyanine (ClAlPc), were obtained through a spontaneous emulsification process based on oil-in-water (o/w) mixtures as described by Primo *et al.*[27] which consists in the formation of emulsification in two stages, initially by the homogenization process by stirring the system, and subsequently reaching the final emulsification stage after removal of the solvent under reduced pressure.[27] The surface-functionalized MNPs investigated in this study (citrate-coated magnetite) were obtained by chemical condensation of aqueous ions (iron cations) in alkaline medium in a first step, following surface-coating treatment with citric acid as described in the literature.[46] X-ray diffraction (XRD) data recorded from the as-produced citrate-coated maghemite-based sample (not shown here) confirmed the iron oxide phase (maghemite) and revealed a mean particle size of 10.4 nm and have been extensively used and previously characterize. Quantification of the incorporated ClAlPc within the as-produced MNE/ClAlPc samples (nanoemulsions loaded with magnetic nanoparticle plus chloroaluminum phthalocyanine).[47]

In the o/w mixture the oil phase consisted of a mixed of organic solvents (high purity grade) prepared from medium-chain triglycerides at 0.75% m/v, natural soy phospholipids (Lipoid S100, Lipid Co., Ribeirão Preto, SP, Brazil) and the PS-drug ClAlPc at 0.5 mg mL^{-1} (Sigma-Aldrich Co., St. Louis, MO, USA) while keeping the temperature set at 55 °C. Subsequently, this organic solution was added into the aqueous phase containing an anionic surfactant, poloxamer 188 (Sigma-Aldrich Co., St. Louis, MO, USA) and different contents of MNPs (0.15×10^{16} or 1.50×10^{16} particle per mL) for each batch. In the last step of the magnetic nanoemulsion (MNE/ClAlPc) preparation the organic solvent was thoroughly removed by rota-evaporation under reduced pressure, at 60 °C.

After preparation of the MNE/ClAlPc samples (0.15×10^{16} or 1.50×10^{16} MNP per mL) steady-state spectroscopic studies were performed using the double beam Lambda 20 Perkin Elmer spectrophotometer in the ultraviolet-visible (UV-VIS), with an option for temperature control and magnetic stirring.[27] All optical spectra obtained in the photophysical studies were exported and formatted using Igor-Pro® software (Wavemetrics 3.16). To assess the mean hydrodynamic particle size, size polydispersity index (PdI) and zeta potential the as-produced MNE/ClAlPC samples were analyzed in the Zetasizer model Nano ZS90 Malvern operating at 633 nm and set to detect at a scattering angle of 90°.[27,48] The assessed data were expressed as a mean ± standard deviation from at least three different batches of each formulation. The measurements were performed at a constant pH of 7.1, as determined by the instrument.

Morphological characteristics of the nanoemulsion

Morphological features of the as-prepared nanoemulsions were evaluated by transmission electronic microscopy (TEM), using a Morgagni 268E FEI instrument operating at 70 kV. First, aliquots of the MNE/ClAlPC samples were prepared by ultracentrifugation at 20.000 rpm for 60 min and the pellets were treated with cacodylate buffer at 1.0 mmol L^{-1}. The samples were centrifuged again at 4.000 rpm and suspended in glutaraldehyde 2% and osmium 2%. Finally, the samples were fixed in spurs and fractioned into microsections for TEM analysis.[49] The laminar material was deposited directly onto the microplates.

Cell cultures

The human mesenchymal stem cells derived from bone marrow (BM-MSC) were cultivated in alpha-modified Minimum Essential Medium (α-MEM; Gibco BRL, USA). The human glioma cell

lines (tumorigenic: U87MG and non-tumorigenic: T98G) (American Type Culture Collection, ATCC, Manassas, VA) were cultivated in Dulbecco's Modified Eagle's Medium-Low (DMEM-LG; Gibco BRL, USA). All the cell lines were supplemented with glutamine 2 mmol L^{-1}, penicillin 100 U mL^{-1}, streptomycin 0.1 mg mL^{-1} and 10% fetal bovine serum (FBS; all from Sigma) at 37 °C and 5% CO_2. Cell micrographs were obtained using a Carl Zeiss microscope Axiovert 40-CFL coupled with a digital high-resolution camera model Axiocam MRC.

Uptake of the photosensitive drug nanocarrier

For subcellular localization experiments, about 2×10^4 cells were carefully added under glass coverslips (13 mm) previously placed at the bottom of each well. The cells were cultured for 24 h (37 °C and 5% CO_2) and then treated with the MNE/ClAlPc samples while untreated cells were used as a control. Incubation with the MNE/ClAlPc samples lasted for about 3 h. Next, the cells were washed twice with Hank's solution and fixed with 2% paraformaldehyde diluted in PBS (Phosphate Buffered Saline) at pH 7.4 (NaCl 137 mM L^{-1}; Na_2HPO_4 10 mM L^{-1}; KH_2PO_4 2 mM L^{-1}; KCl 2.7 mM L^{-1}) for 20 min. After fixation, the cells were washed five times for 3 min with PBS containing glycine 100 mM and permeabilized with 0.1% Triton X-100 diluted in PBS over a period of 10 min. After permeabilization, the cells were washed five times for 5 min with PBS. Then, the coverslips containing the adhered cells were removed out from the wells and mounted onto glass slides containing ProLong Gold antifade reagent containing DAPI (4′,6-diamidino-2-phenylindole) and mounting medium (Thermo Fisher Scientific, USA), followed by incubation for 20 min. The slides were observed under a Leica TCS-SP5 confocal laser-scanning microscope (Leica Microsystems, Mannheim, Germany). The ClAlPc was detected using a 633 HeNe laser with excitation/emission (641/780 nm), GFP (green fluorescent protein) was detected with an Argon laser (488/540 nm) whereas DAPI was detected with a diode laser (358/461 nm).

Hyperthermia and photodynamic therapies

The equipment used to apply the external AC magnetic field during the HPT studies operated at 1 MHz with 40 Oe magnetic field amplitude and was developed at the Institute of Biological Sciences, University of Brasília (Brasília, Brazil). The PDT protocol used a typical diode laser set at 670 nm (Eagle Laser, Quantum Tech, São Carlos, Brazil) at a difference fluencies rate from 100, 200, and 700 mJ cm^{-2} with a power density of 56, 7 mW cm^{-2}. The spot where setup to 1.5 cm^2 to cover the hole cell culture plate. For different treatments the cell viability was assessed by the MTT test ([3-(4,5-dimethylthiazol-2-yl)-2,5-diphenyl tetrazolium bromide]).[42]

Statistical analysis

Statistical analyses of the cell viability assays – MTT were generated within the GraphPad Prism 6.0 (GraphPad Software, Inc.) platform. Differences between control and treated groups were evaluated using analysis of variance (ANOVA) followed by Tukey test (significance was set at $P < 0.05$).

Conclusions

The present study reports on the production of two formulations of magnetic nanoemulsions (MNEs) with the average mean size of around 200 nm, comprising encapsulation of citrate-coated maghemite nanoparticles (XRD data: mean particle size of 10.4 nm from) at 0.15×10^{16} or 1.50×10^{16} particle per mL plus chloroaluminum-phthalocyanine (0.05 mg mL^{-1}). Compared to previous formulations and studies the two new formulations increased the content of both the magnetic nanoparticle by three orders of magnitude and the chloroaluminum-phthalocyanine by one order of magnitude. Three different cell line models (BM-MSC, U87MG, and T98G) were used to assess the cell viability (MTT test) while incubating the cells with the two prepared formulations, as opposed to the previous study using just one cell line, and thereby representing a more comprehensive investigation. The *in vitro* studies were conducted before and after performing hyperthermia (HPT: 1 MHz frequency, 40 Oe magnetic field amplitude) and photodynamic therapy (PDT at 670 nm wavelength, 700 mJ cm^{-2} energy density). From the present study we found that the HPT treatment reduces the cell viability in to about 15%, regardless the magnetic nanoparticle content within the MNE. An enhanced cytotoxicity was observed while using both MNE formulations to perform the PDT treatment, from which we found the cell viability decreasing down to about 52%. However, a superior reduction in cell viability of about 70% was found while combining the HPT and PDT treatments. Moreover, confocal microscopy images clearly indicated the cytoplasm localization and active site of the as-prepared drug delivery device. Therefore, we envisage that the combined treatment of HPT and PDT represents a promising paradigm for brain cancer intervention, such as glioblastoma.

Acknowledgements

The authors would like to acknowledge the Foundation for the State of São Paulo Research – FAPESP (Post.Doc Project # 2015/18684-9 L.B.P; Thematic Project # 2013/50181-1 FINEP Project 01.10.0758.01 and CNPq-National Institute of Science and Technology (INCT) of Nanobiotechnology project 573880/2008-5 A.C.T.) for the financial support.

References

1 F. B. Furnari, T. Fenton, R. M. Bachoo, A. Mukasa, J. M. Stommel, A. Stegh, W. C. Hahn, K. L. Ligon, D. N. Louis and C. Brennan, *Genes Dev.*, 2007, **21**, 2683–2710.
2 O. O. Kanu, A. Mehta, C. Di, N. Lin, K. Bortoff, D. D. Bigner, H. Yan and D. C. Adamson, *Expert Opin. Ther. Targets*, 2009, 701–718.
3 M. S. S. Bovenberg, M. H. Degeling and B. A. Tannous, *Trends Mol. Med.*, 2013, **19**, 281–291.
4 R. Stupp, W. Mason and M. van den Beuf, *Annals of Oncology*, 2005, **16**, 949.

5 X.-Y. Li, Y. Zhao, M.-G. Sun, J.-F. Shi, R.-J. Ju, C.-X. Zhang, X.-T. Li, W.-Y. Zhao, L.-M. Mu and F. Zeng, *Biomaterials*, 2014, **35**, 5591–5604.
6 M. Cruz, Å. Siden, D. Tasat and J. Yakisich, *J. Cancer Sci. Ther.*, 2010, **2**, 100–106.
7 S. K. Singh, I. D. Clarke, M. Terasaki, V. E. Bonn, C. Hawkins, J. Squire and P. B. Dirks, *Cancer Res.*, 2003, **63**, 5821–5828.
8 W. Guo, J. L. Lasky and H. Wu, *Pediatr. Res.*, 2006, **59**, 59R–64R.
9 I. Lasky, L. Joseph, M. Choe and I. Nakano, *Curr. Stem Cell Res. Ther.*, 2009, **4**, 298–305.
10 K. M. Joo, S. Y. Kim, X. Jin, S. Y. Song, D.-S. Kong, J.-I. Lee, J. W. Jeon, M. H. Kim, B. G. Kang and Y. Jung, *Lab. Invest.*, 2008, **88**, 808–815.
11 Y. N. Konan, R. Gurny and E. Allémann, *J. Photochem. Photobiol., B*, 2002, **66**, 89–106.
12 E. Da Rocha, L. Porto and C. Rambo, *Mater. Sci. Eng., C*, 2014, **34**, 270–279.
13 D. Peer, J. M. Karp, S. Hong, O. C. Farokhzad, R. Margalit and R. Langer, *Nat. Nanotechnol.*, 2007, **2**, 751–760.
14 K. Y. Choi, G. Liu, S. Lee and X. Chen, *Nanoscale*, 2012, **4**, 330–342.
15 X. Dong and R. J. Mumper, *Nanomedicine*, 2010, **5**, 597–615.
16 A. Gupta, H. B. Eral, T. A. Hatton and P. S. Doyle, *Soft Matter*, 2016, **12**, 2826–2841.
17 L. Wang, K. J. Mutch, J. Eastoe, R. K. Heenan and J. Dong, *Langmuir*, 2008, **24**, 6092–6099.
18 C. Solans, P. Izquierdo, J. Nolla, N. Azemar and M. Garcia-Celma, *Curr. Opin. Colloid Interface Sci.*, 2005, **10**, 102–110.
19 W. D. Jang, N. Nishiyama, G. D. Zhang, A. Harada, D. L. Jiang, S. Kawauchi, Y. Morimoto, M. Kikuchi, H. Koyama and T. Aida, *Angew. Chem.*, 2005, **117**, 423–427.
20 M.-J. Rang and C. A. Miller, *J. Colloid Interface Sci.*, 1999, **209**, 179–192.
21 M. Rang and C. Miller, in *Horizons 2000–aspects of colloid and interface science at the turn of the millenium*, Springer, 1998, pp. 101–117.
22 T. Nishimi and C. A. Miller, *J. Colloid Interface Sci.*, 2001, **237**, 259–266.
23 J. Gutiérrez, C. González, A. Maestro, I. Sole, C. Pey and J. Nolla, *Curr. Opin. Colloid Interface Sci.*, 2008, **13**, 245–251.
24 J. Chen, M. Yang, Q. Zhang, E. C. Cho, C. M. Cobley, C. Kim, C. Glaus, L. V. Wang, M. J. Welch and Y. Xia, *Adv. Funct. Mater.*, 2010, **20**, 3684–3694.
25 G. Von Maltzahn, J.-H. Park, K. Y. Lin, N. Singh, C. Schwöppe, R. Mesters, W. E. Berdel, E. Ruoslahti, M. J. Sailor and S. N. Bhatia, *Nat. Mat.*, 2011, **10**, 545–552.
26 K. Nagahama, T. Utsumi, T. Kumano, S. Maekawa, N. Oyama and J. Kawakami, *Sci. Rep.*, 2016, 30962.
27 F. L. Primo, M. Rodrigues, A. R. Simioni, Z. G. Lacava, P. C. Morais and A. C. Tedesco, *J. Nanosci. Nanotechnol.*, 2008, **8**, 5873–5877.
28 R. Tietze, S. Lyer, S. Dürr and C. Alexiou, *Nanomedicine*, 2012, **7**, 447–457.
29 G. C. Bolfarini, M. P. Siqueira-Moura, G. J. Demets, P. C. Morais and A. C. Tedesco, *J. Photochem. Photobiol., B*, 2012, **115**, 1–4.
30 G.-q. Yi, B. Gu and L.-k. Chen, *Tumor Biol.*, 2014, **35**, 2445–2449.
31 M. Zaki, F. Arjmand and S. Tabassum, *Inorg. Chim. Acta*, 2016, **444**, 1–22.
32 K. Ahmed, Y. Tabuchi and T. Kondo, *Apoptosis*, 2015, **20**, 1411–1419.
33 A. Master, M. Livingston and A. S. Gupta, *J. Controlled Release*, 2013, **168**, 88–102.
34 M. O. Dereski, L. Madigan and M. Chopp, *Neurosurgery*, 1995, **36**, 141–146.
35 H. Hirschberg, C.-H. Sun, B. J. Tromberg, A. T. Yeh and S. J. Madsen, *J. Neuro-Oncol.*, 2004, **70**, 289–299.
36 S. Shrestha, P. Jiang, M. H. Sousa, P. C. Morais, Z. Mao and C. Gao, *J. Mater. Chem. B*, 2016, **4**, 245–256.
37 L. B. de Paula, F. L. Primo, M. R. Pinto, P. C. Morais and A. C. Tedesco, *J. Magn. Magn. Mater.*, 2015, **380**, 372–376.
38 E. Silva, L. Franchi and A. Tedesco, *RSC Adv.*, 2016, **6**, 79631–79640.
39 B. Lamas, B. Abreu, A. Fonseca, N. Martins and M. Oliveira, *J. Colloid Interface Sci.*, 2012, **381**, 17–23.
40 W.-Y. Cheng, M.-T. Chiao, Y.-J. Liang, Y.-C. Yang, C.-C. Shen and C.-Y. Yang, *Mol. Biol. Rep.*, 2013, **40**, 5315–5326.
41 J. M. Dąbrowski, B. Pucelik, A. Regiel-Futyra, M. Brindell, O. Mazuryk, A. Kyzioł, G. Stochel, W. Macyk and L. G. Arnaut, *Coord. Chem. Rev.*, 2016, **325**, 67–101.
42 T. Mosmann, *J. Immunol. Methods*, 1983, **65**, 55–63.
43 L. Wang, W. Zhao and W. Tan, *Nano Res.*, 2008, **1**, 99–115.
44 L. A. Muehlmann, B. C. Ma, J. P. F. Longo, M. F. M. A. Santos and R. B. Azevedo, *Int. J. Nanomed.*, 2014, **9**, 1199.
45 P. Severino, J. Fangueiro, S. Ferreira, R. Basso, M. Chaud, M. Santana, A. Rosmaninho and E. Souto, *Clin. Transl. Oncol.*, 2013, **15**, 417–424.
46 S. Da Silva, T. Melo, M. Soler, E. Lima, M. Da Silva and P. Morais, *IEEE Trans. Magn.*, 2003, **39**, 2645–2647.
47 M. Siqueira-Moura, F. Primo, A. Peti and A. Tedesco, *Die Pharmazie*, 2010, **65**, 9–14.
48 F. Primo, M. da Costa Reis, M. Porcionatto and A. Tedesco, *Curr. Med. Chem.*, 2011, **18**, 3376–3381.
49 M. P. Siqueira-Moura, F. L. Primo, E. M. Espreafico and A. C. Tedesco, *Mater. Sci. Eng., C*, 2013, **33**, 1744–1752.

